Pakistan Veterinary Journal

ISSN: 0253-8318 (PRINT), 2074-7764 (ONLINE)
DOI: 10.29261/pakvetj/2026.018

RESEARCH ARTICLE

Lentivirus-driven Hematopoietic Prostaglandin D Synthase Overexpression Exerts a Negative Regulatory Effect on the Corpus Luteum in Sheep

Heng Yang[1#*], Rui Lin[#1], Jiamin Wu[#1], Lianghui Long[1], Licai Li[1], Huihao Xu[1], Zhengkai Wei[1], Ling Gan[1], Gaofu Wang[2], Lin Fu[2*] and Xianwen Dong[2*]

[1]College of Veterinary Medicine, Southwest University, Chongqing 402460, China; [2]Chongqing Academy of Animal Sciences, Chongqing 402460, China. [#]These authors contributed equally to this study.
*Corresponding author: yhuv2013@sina.com (HY); lyfl1990@163.com (LY); dongxw20220722@gmail.com (XD)

ARTICLE HISTORY (25-1009)

Received: October 25, 2025
Revised: January 03, 2026
Accepted: January 05, 2026
Published online: February 25, 2026

Key words:
Apoptosis
HPGDS
Luteal cells
Progesterone
qRT-PCR
Receptor type

ABSTRACT

The maintenance and regression of corpus luteum are regulated by prostaglandin $F_{2\alpha}$, but the role of prostaglandin D_2 (PGD_2) has not been thoroughly investigated. Its synthesis involves the key enzyme, hematopoietic prostaglandin D synthase (HPGDS) that mediates PGD_2 production in different cell types. The aim of this study was to investigate the biological role of endogenous PGD_2 on luteal cells in *Hu* sheep via HPGDS overexpression. For this purpose, luteal cells obtained from luteal tissue of 5 healthy adult *Hu* sheep at the mid-luteal phase immediately after slaughter were isolated via mechanical dissociation, enzymatic digestion, and Percoll density gradient centrifugation, cryopreserved in liquid nitrogen, and retrieved for subsequent experiments. Subsequently, quantitative real-time PCR (qRT-PCR) was used to confirm the efficiency of HPGDS overexpression. ELISA, qRT-PCR and Western blot (WB) were utilized to detect key indicators of luteal function and structural regression. Immunofluorescence was used to localize the PGD_2 receptors. Analytical results of lentiviral construction showed that HPGDS lentiviral plasmids were constructed, packaged in 293T cells, with MOI of 160 determined as optimal for luteal cell infection. HPGDS overexpression reduced P_4 concentration and StAR expression ($P<0.01$), showing impaired luteal endocrine function. Meanwhile, it increased BAX mRNA and protein and BAX/BCL-2 protein ratio ($P<0.01$), indicating enhanced luteal cell apoptosis. Moreover, HPGDS overexpression raised ROS concentration ($P<0.01$), upregulated mRNA levels of ATP6V1B1, SLCO2A1, PRKCE, and DP1 ($P<0.01$), while downregulating mRNA level of CREB ($P<0.01$), with enhanced DP1 fluorescence intensity. These findings indicate that HPGDS overexpression impairs progesterone secretion and promotes luteal cell apoptosis, suggesting that PGD_2 negatively regulates CL lifespan in small ruminants through HPGDS-related pathways.

To Cite This Article: Yang H, Lin R, Wu J, Long L, Li L, Xu H, Wei Z, Gan L, Wang G, Fu L and Dong X, 2026. Lentivirus-driven hematopoietic prostaglandin d synthase overexpression exerts a negative regulatory effect on the corpus luteum in sheep. Pak Vet J. http://dx.doi.org/10.29261/pakvetj/2026.018

INTRODUCTION

In mammals, the corpus luteum (CL) is a transient endocrine gland that develops from ovarian granulosa and theca cells remaining in the follicle after ovulation. It secretes progesterone (P_4), necessary for controlling the reproductive cycle, fertility and pregnancy maintenance (de Souza *et al.,* 2024). Disruption of CL formation or regression during the normal estrous cycle can directly affect estrous cyclicity, adversely affecting reproductive efficiency of the female (Wiltbank *et al.,* 2018). Therefore, the CL is a key component in reproductive control of mammals, and its formation and timely regression is a prerequisite for successful reproduction.

Hormonal regulation is involved in the reproductive cycle through autocrine and paracrine mechanisms, with important roles played by prostaglandins (PGs), a family of structurally related eicosanoids (Berisha *et al.,* 2018). Among members of this family, PGE_2 and $PGF_{2\alpha}$ are particularly important and have been extensively studied in reproductive biology (Berisha *et al.,* 2018; Tippenhauer *et al.,* 2021; Tavakolikazerooni *et al.,* 2025). Generally, $PGF_{2\alpha}$ is the key PG that causes luteal regression (Tavakolikazerooni *et al.,* 2025), whereas PGE_2 is

necessary to maintain CL (Pate and Hughes, 2023). When PGE_2 secretion reaches peak levels in pregnant mammals, it suppresses the transformation of PGH_2 to $PGF_{2\alpha}$ (Ochoa *et al.,* 2018, Satoh *et al.,* 2021; Pate and Hughes, 2023), significantly lowering uterine $PGF_{2\alpha}$ and thus enhancing CL growth and fetal development during gestation (Ochoa *et al.,* 2018). The balance between PGE_2 and $PGF_{2\alpha}$ is necessary for a successful pregnancy, as it maintains CL stability and ensures P_4 production. This regulatory system weakens near parturition, causing pregnancy-maintaining CL to regress (Ochoa *et al.,* 2018; Pate and Hughes, 2023). Due to PGE_2 depletion, PGH_2 conversion enhances $PGF_{2\alpha}$ production, which facilitates functional (depleting P_4 level) and structural (weakening CL structure and volume loss) regression in postpartum and cyclic females, eventually triggering a new reproductive cycle.

Another PG family member, prostaglandin D_2 (PGD_2), has received attention in recent years. The PGD_2 is widely distributed in mammalian tissues and participates in physiological processes, including inflammatory responses (Gong *et al.,* 2023), sleep promotion (Ahmad *et al.,* 2019), nociception (Li *et al.,* 2021) and chronic asthma (Ullah *et al.,* 2024). In reproduction, studies have shown that PGD_2 can induce vascular relaxation and thereby increase blood flow in the utero-ovarian vascular system (Bonnin *et al.,* 1999; Charpigny *et al.,* 1999), suggesting that PGD_2 enhances $PGF_{2\alpha}$ delivery to the CL. This augmented blood circulation can enhance the luteolytic action of $PGF_{2\alpha}$, resulting in accelerated and complete CL regression (Neglia *et al.,* 2012). This synergistic effect of PGD_2 in CL regression is not well understood and needs additional experimental support.

In mammals, the primary synthase of PGD_2 is the sigma class glutathione transferase, hematopoietic prostaglandin D synthase (HPGDS). The aim of this study was to investigate the role of PGD_2 in regulating the lifespan of ovine luteal cells by means of HPGDS overexpression. This is expected to provide new insights into the biological effects of PGD_2 in reproduction, thereby laying a solid foundation for refining the molecular network mechanism through which the members of the PG family regulate CL regression.

MATERIALS AND METHODS

Cell culture: Experiments relating to this study were conducted at the Key Laboratory of Herbivorous Livestock (Southwest University) and the Institute of Herbivorous Livestock (Chongqing Academy of Animal Sciences), China, during the period from September to November, 2023. The 293T cells stably express the SV40 large T antigen, which facilitates efficient replication of episomal vectors containing the SV40 origin of replication (e.g., lentiviral vectors) (Abaandou *et al.,* 2021), and are therefore widely used in lentivirus packaging. These cells were supplied by Fenghui Biotechnology Co., Ltd., China. These 293T cells were thawed rapidly at 37°C, centrifuged (1000rpm, 5min), resuspended in DMEM/F12, and cultured in a 37°C CO_2 incubator.

For the isolation of large luteal cells (LLC), CLs were obtained from the ovaries of 5 healthy adult *Hu* sheep at the mid-luteal phase (6-9 days post-ovulation), where ovaries were collected immediately after slaughter, transported to the laboratory in sterile phosphate-buffered saline (PBS), and dissected to isolate CL tissues. Minced CL fragments were enzymatically digested into a single-cell suspension, purified via trypsin-induced differential centrifugation and Percoll density gradient centrifugation (final purity >90%), and verified by immunocytochemical staining for synaptophysin and 3β-hydroxysteroid dehydrogenase (Yang *et al.,* 2023). At this point, these LLC were revived, cultured in DMEM/F12 with 10% FBS at 37°C, 5% CO_2. They were then seeded in 96-well plates (100μL/well, 24, 48 and 72h were set as experimental groups, each inoculated with cells, 5 replicates/group) with a blank control (medium only). At 24, 48 and 72h post-revival, 10μL CCK-8 was added; absorbance at 450nm was measured after 2h, and cell viability was calculated (Han *et al.,* 2022). Experiments were conducted in triplicate.

Viral vectors and packaging and harvesting of lentiviruses: HPGDS cDNA was cloned into the pLV-CMV vector to construct recombinant plasmid pLV-CMV-HPGDS. For plasmid identification, the recombinant construct was double-digested with EcoRI and BamHI, and the products were analyzed by 1% agarose gel electrophoresis. Plasmids displaying the expected restriction profiles were submitted to Tsingke Biotech Co., Ltd (Beijing, China) for sequencing, and the resulting data were verified using DNAMAN software. Cultures of confirmed positive clones were then scaled up and stored as glycerol stocks at -80°C. The 293T cells (80-90% confluent) were transfected with pLV-CMV (empty) or pLV-CMV-HPGDS. Culture medium was centrifuged (4°C, 4000rpm, 10min), supernatant was re-centrifuged (20,000rpm, 30min), the pellet was resuspended in phosphate buffered saline (PBS, 1mL), and re-centrifuged (10,000rpm, 10min); final supernatant was stored at -80°C (Chen *et al.,* 2018; Chen *et al.,* 2024). The viral titers (TU/mL) were determined via 10-fold serial dilution in 293T cells (1×10^4/well), with fluorescence observed after 24h, using the following formula:

Titer (TU/mL) = Cells × fluorescence(%) × 10/virus volume (μL).

Optimal multiplicity of infection (MOI) selection and lentivirus transfection: Large luteal cells (1×10^5/mL) in 96-well plates were infected with MOIs 40-240 (Table 1). After 24h, medium was replaced; and the fluorescence was examined at 72h. The MOI with >80% infection efficiency and high viability was selected. Large luteal cells in 6-well plates (70% confluent) were divided into blank control (BC, without virus), empty vector (pLV-CMV lentivirus), and HPGDS (pLV-CMV-HPGDS lentivirus) groups, with four replicates per group. Virus was added per optimal MOI. At 72h, fluorescence was observed, and HPGDS expression was analyzed by qRT-PCR, as described earlier (Wang *et al.,* 2022).

Progesterone level detection: Progesterone level in culture medium was measured via ELISA. The lower limit of detection was 0.05ng/mL; intra-assay CV was ≤10%, and inter-assay CV was ≤12% (Jiangsu Jingmei Biotechnology Co., Ltd, China; Zhu *et al.,* 2025).

Table 1: Volume of virus liquid added to the plates at different multiplicity of infection (MOI) values per well

Number of cells	MOI value	pLV-CMV-HPGDS virus titer (TU/mL)	Volume of pLV-CMV-HPGDS virus liquid (μL)	pLV-CMV virus titer (TU/mL)	Volume of pLV-CMV virus liquid(μL)
1×10^4	40	1.4×10^8	2.8	1.0×10^8	4.0
1×10^4	80	1.4×10^8	5.6	1.0×10^8	8.0
1×10^4	120	1.4×10^8	8.6	1.0×10^8	12.0
1×10^4	160	1.4×10^8	11.4	1.0×10^8	16.0
1×10^4	200	1.4×10^8	14.3	1.0×10^8	20.0
1×10^4	240	1.4×10^8	17.1	1.0×10^8	24.0

Note: The amount of virus added per well (μL) = MOI × number of cells/virus titer (TU/mL) ×1000

qRT-PCR and Western blot: Total RNA was extracted via TRIzol reagent (Thermo Fisher Scientific, Cat. 15596026), with quality verified by 1% agarose gel electrophoresis and NanoDrop analysis (A260/280=1.8-2.0). Next, the validated RNA was used to synthesize cDNA via PrimeScript™ RT Master Mix (Takara Biomedical Technology Co., Ltd., Cat. RR036A). qRT-PCR was run on a QuantStudio 6 Flex Real-Time system (Thermo Fisher Scientific, USA) with TB Green® Premix Ex Taq™ (Takara Biomedical Technology Co., Ltd., Cat. RR820A). 10μL reaction mixture contained 5μL 2× Premix, 0.4μL each primer (10μM), 1μL cDNA, 0.2μL 50× ROX Reference Dye, and 3.0μL nuclease-free water. Cycling conditions were: 95°C (30s) pre-denaturation, 40 cycles of 95°C (5s) and 60°C (30s), as described earlier (Fang *et al.,* 2022). Each sample had 3 biological and 3 technical replicates. Primer information is shown in Table 2. Proteins from LLC were extracted via RIPA, quantified by BCA, separated by SDS-PAGE, and transferred to PVDF membranes. Membranes were then probed with BAX/BCL-2/β-actin primary antibodies (4°C overnight), and then with HRP-conjugated secondary antibody. Bands were visualized via ECL and quantified with Quantity One (Wang *et al.,* 2025).

Table 2: QRT-PCR primers used in the study

Gene name	Product size (bp)	Primer sequences（5'-3'）	GenBank accession No.
HPGDS	221	F: GGCTGGAAAAACAGAACTTGA R: AGTCTGCCCAAGTTACAGAGTC	XM_004009700.6
StAR	115	F: CCACACTCTACGAGGAGAT R: CAGGTGAGTTTGGTCCTTG	XM_060406892.1
BCL-2	152	F: TTCGCCGAGATGTCCAG R: ACGCTCTCCACACACATGAC	XM_012103831.5
BAX	158	F: CTACTTTGCCAGCAAACTGG R: TCCCAAAGTAGGAGAGGA	XM_027978593.3
CREB	163	F: CTGGGGTTGTTATGGCGTCT R: AGCACTGCCACTCTGTTCTC	XM_015093513.4
SLCO2A1	165	F: CGCCCCTGTACATCTCCATC R: ACCACCAGGCTCCTATCCAT	NM_001038021.1
PRKCE	62	F: CTCATTGCTGGTGCTGAGTC R: CGATCTTCCTCAGACGGTGA	XM_060412213.1
ATP6V1B1	96	F: CTCAGCGGAGTGGGCAAGTG R: AGGTGGTCTTCTGGGCATCAATC	XM_004006053.6
CRTH2	182	F: GCTGCGGCCCACAAGGTCT R: AGGGCCGTCTGGCGCGAGT	XM_042237708.1
DP1	115	F: TTCAGCACAGCAACAAGCT R: ATCTTACCATCTCCACCAA	XM_027971746.3
β-actin	104	F: CCAAGGCCAACCGTGAGAAG R: GCCAGAGGCGTACAGGGACA	NM_001009784.3

Note: F: Forward primer; R: Reverse primer.

Immunofluorescence detection: Large luteal cells were fixed (4% paraformaldehyde), permeabilized (0.25% Triton X-100), blocked (1% BSA), and incubated with PGD_2 receptor 1 (DP1) and receptor 2 (CRTH2; chemoattractant receptor-homologous molecule expressed on Th2 cells) primary antibodies (4°C overnight). FITC-conjugated secondary antibodies and 4',6-diamidino-2-phenylindole (DAPI) were applied; finally, fluorescence intensity was analyzed via Image J.

Statistical analysis: QRT-PCR data were analyzed using $2^{-\Delta\Delta Ct}$, and cell viability data were analyzed using optical density (OD) values (Tan et al., 2020). Statistical analyses were performed using SPSS 22.0 software. One-way analysis of variance (ANOVA) with appropriate post-hoc tests was used for intergroup comparisons. $P<0.01$ was denoted with **(highly significant difference) and $P<0.05$ was denoted with *(significant difference).

RESULTS

Enzyme digestion and sequencing confirmation of recombinant vectors and lentivirus packaging: Fig. 1A shows the agarose gel electrophoresis results of the pLV-CMV-HPGDS plasmid digested with EcoRI and BamHI. Two distinct bands were observed: one approximately at 8814 bp (corresponding to pLV-CMV vector), and another around 600 bp (corresponding to HPGDS insert), which matched the expected fragment sizes. Fig. 1B presents the sequencing alignment between the inserted HPGDS gene in pLV-CMV-HPGDS and the NCBI reference sequence, confirming 100% sequence accuracy. Fig. 1C and D display the bright-field images of 293T cells transfected with pLV-CMV and pLV-CMV-HPGDS, respectively, while Fig. 1E and F show corresponding fluorescence images. Fluorescence signals in both transfection groups confirm efficient transfection and successful packaging of the lentiviral vectors.

Lentiviral titer: The viral titers of pLV-CMV and pLV-CMV-HPGDS lentiviruses were assessed via limiting dilution, followed by infection of 293T cells. Infection efficiency was evaluated using inverted fluorescence microscopy. Fig. 2A shows bright-field and fluorescence images of the pLV-CMV-HPGDS group, while Fig. 2B reflects bright-field and fluorescence images of the pLV-CMV group. The fluorescence intensity indicated that both lentiviruses achieved a titer of approximately 1.4×10^8TU/mL, demonstrating high-quality viral preparations suitable for subsequent experiments.

MOI for lentiviral infection in luteal cells: CCK-8 assay results showed the relative OD values of LLC at 24, 48 and 72h post-resuscitation as 0.31±0.03, 0.56±0.05, and 0.87±0.06, respectively, showing a time-dependent increase (Fig. 3A). Cells exhibited detectable metabolic activity as early as 24h post-resuscitation, and this activity significantly increased at 48h compared to 24h ($P<0.01$), with the highest activity at 72h, indicating good viability of resuscitated luteal cells. Subsequently, luteal cells were infected with pLV-CMV and pLV-CMV-HPGDS at different titers to determine the optimal MOI. Results showed that infection efficiency remained relatively low when the MOI was between 40 and 120, whereas it reached a peak when the MOI was raised to 160 (Fig. 3B). Thus, an MOI of 160 was found to be the optimal for luteal cell infection.

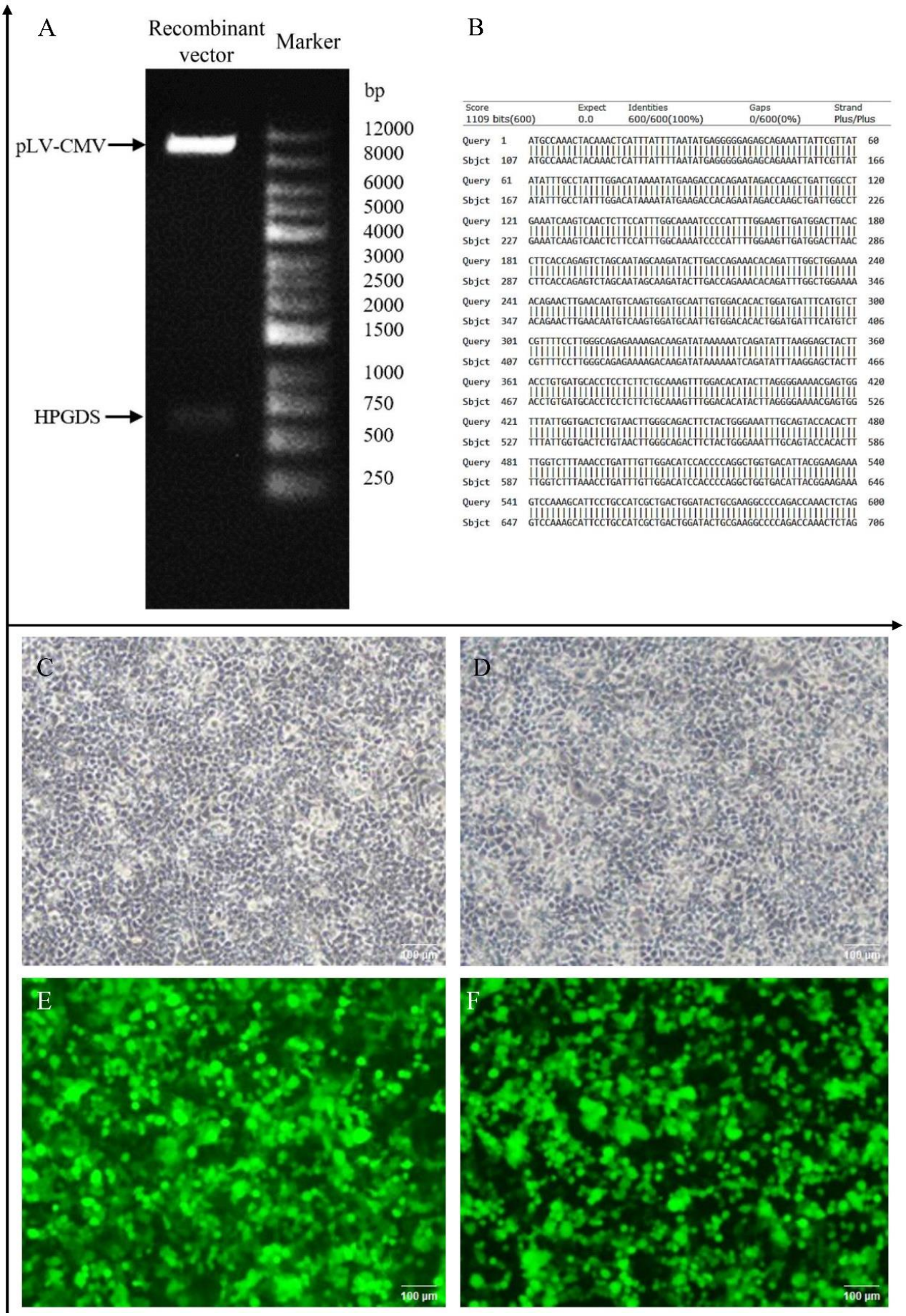

Fig. 1: Double enzyme digestion agarose gel electrophoresis, sequencing and packaging of pLV-CMV-HPGDS lentivirus overexpression vector. A): double enzyme digestion; B): DNA sequencing; C): pLV-CMV white light image; D): pLV-CMV-HPGDS white light image; E): pLV-CMV green fluorescence image; F): pLV-CMV-HPGDS green fluorescence image. Scale bar=100μm.

HPGDS overexpression efficiency in luteal cells: Using the optimal MOI, luteal cells were infected with lentivirus and divided into three specific groups: blank control (BC, no virus), pLV-CMV (empty vector lentivirus), and pLV-CMV-HPGDS (recombinant vector lentivirus). Fig. 4A-C confirm successful transfection of both lentiviruses into luteal cells. The qRT-PCR analysis showed that HPGDS expression in the pLV-CMV-HPGDS group was significantly upregulated compared to the BC and pLV-CMV groups ($P<0.01$; Fig. 4D), confirming successful HPGDS overexpression in luteal cells**.**

Changes in expression levels of key indicators involved in CL functional and structural regression: Compared to the BC group and EVC groups, the HPGDS overexpression group showed a highly significant decrease in P_4 concentration in luteal cells ($P<0.01$; Fig. 5A). Similarly, the relative expression of StAR (a key protein in P_4 synthesis) was highly significantly downregulated in the HPGDS overexpression group compared to BC group and EVC groups ($P<0.01$; Fig. 5B). After HPGDS overexpression, qRT-PCR results showed that pro-apoptotic factor BAX mRNA was highly significantly upregulated compared to BC and EVC groups ($P<0.01$; Fig. 5C), while anti-apoptotic factor BCL-2 mRNA showed non-significant change (Fig. 5D). The WB analysis further confirmed a highly significant upregulation of BAX protein in the HPGDS overexpression group compared to BC group and EVC groups ($P<0.01$; Fig. 5E and F), with no change in BCL-2 protein (Fig. 5E and G). Notably, the BAX/BCL-2 ratio was significantly increased in the HPGDS overexpression group compared to BC group and EVC groups ($P<0.01$; Fig. 5H), indicating a tendency towards apoptosis in HPGDS-overexpressing luteal cells.

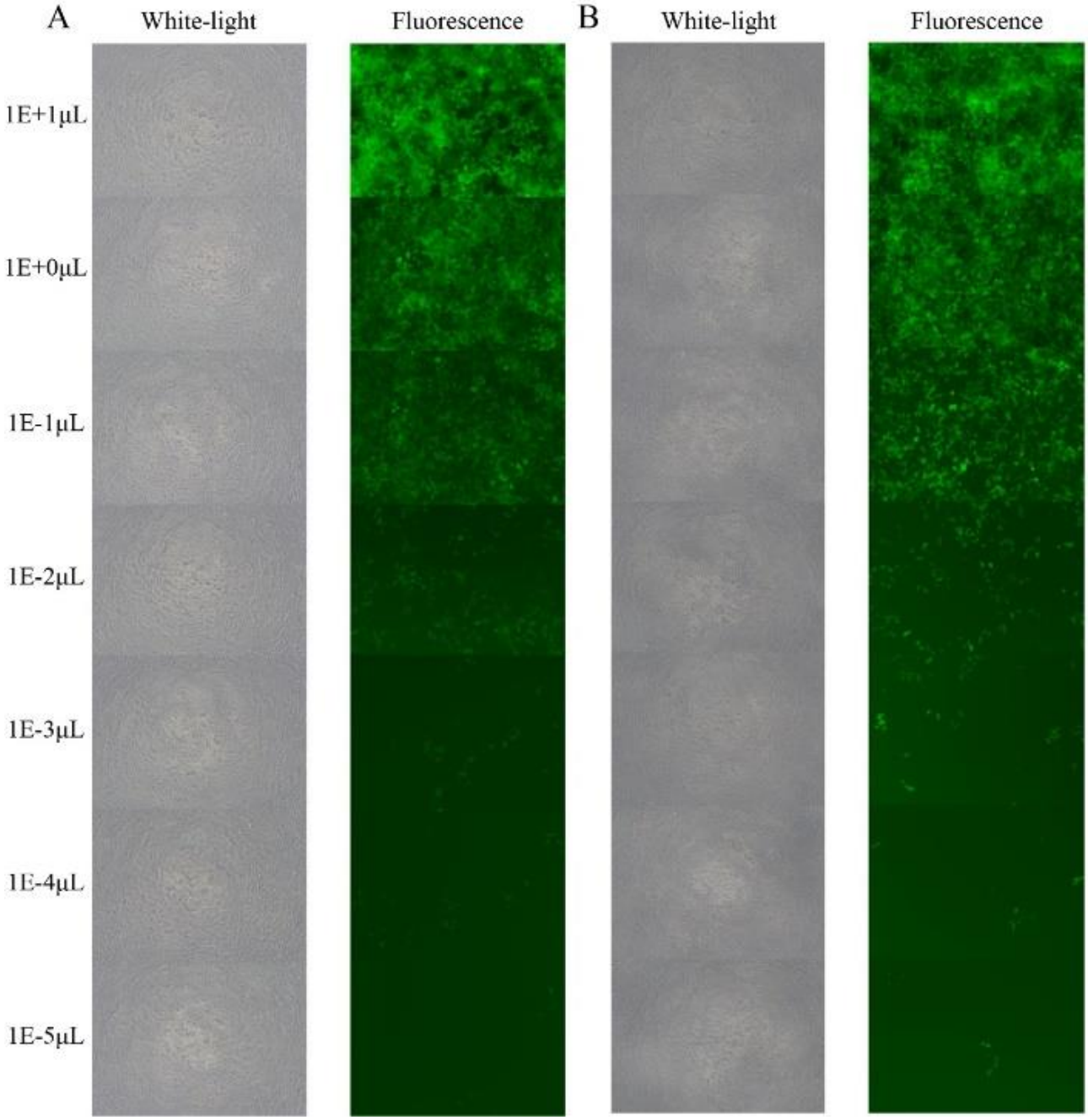

Fig. 2: 293T cells infected with different titers of pLV-CMV-HPGDS and pLV-CMV lentivirus (100×). A): pLV-CMV-HPGDS; B): pLV-CMV.

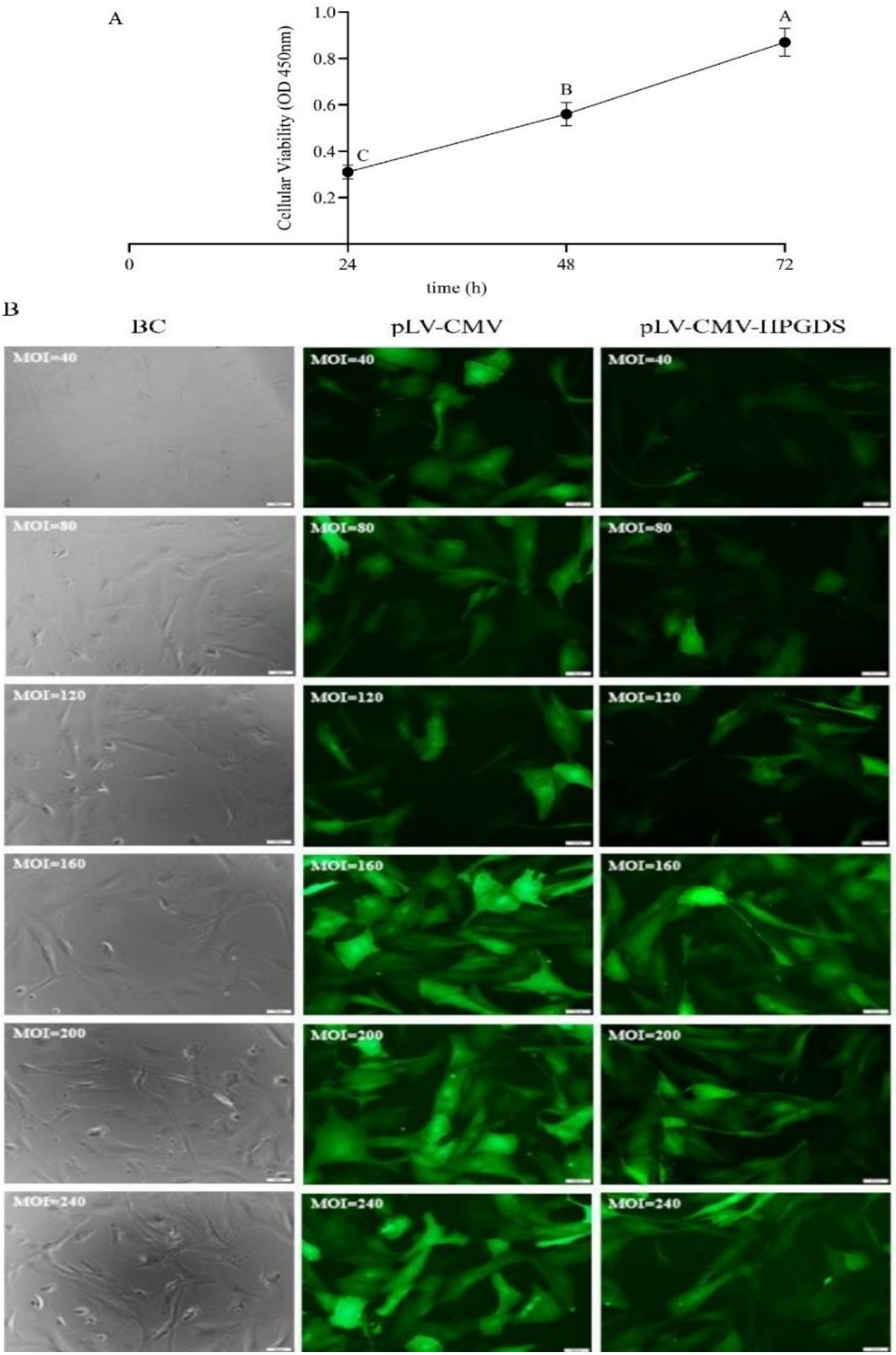

Fig. 3: Cellular viability and the effect of pLV-CMV and pLV-CMV-HPGDS on luteal cells infection at different MOI values. A): the viability of luteal cells assessed by the CCK-8 assay. Different capital letters indicate highly significant differences between groups ($P<0.01$). B): Lentivirus transfection efficiency of luteal cells observed by fluorescence microscope (100×). The positive transfected cells are shown in green fluorescence.

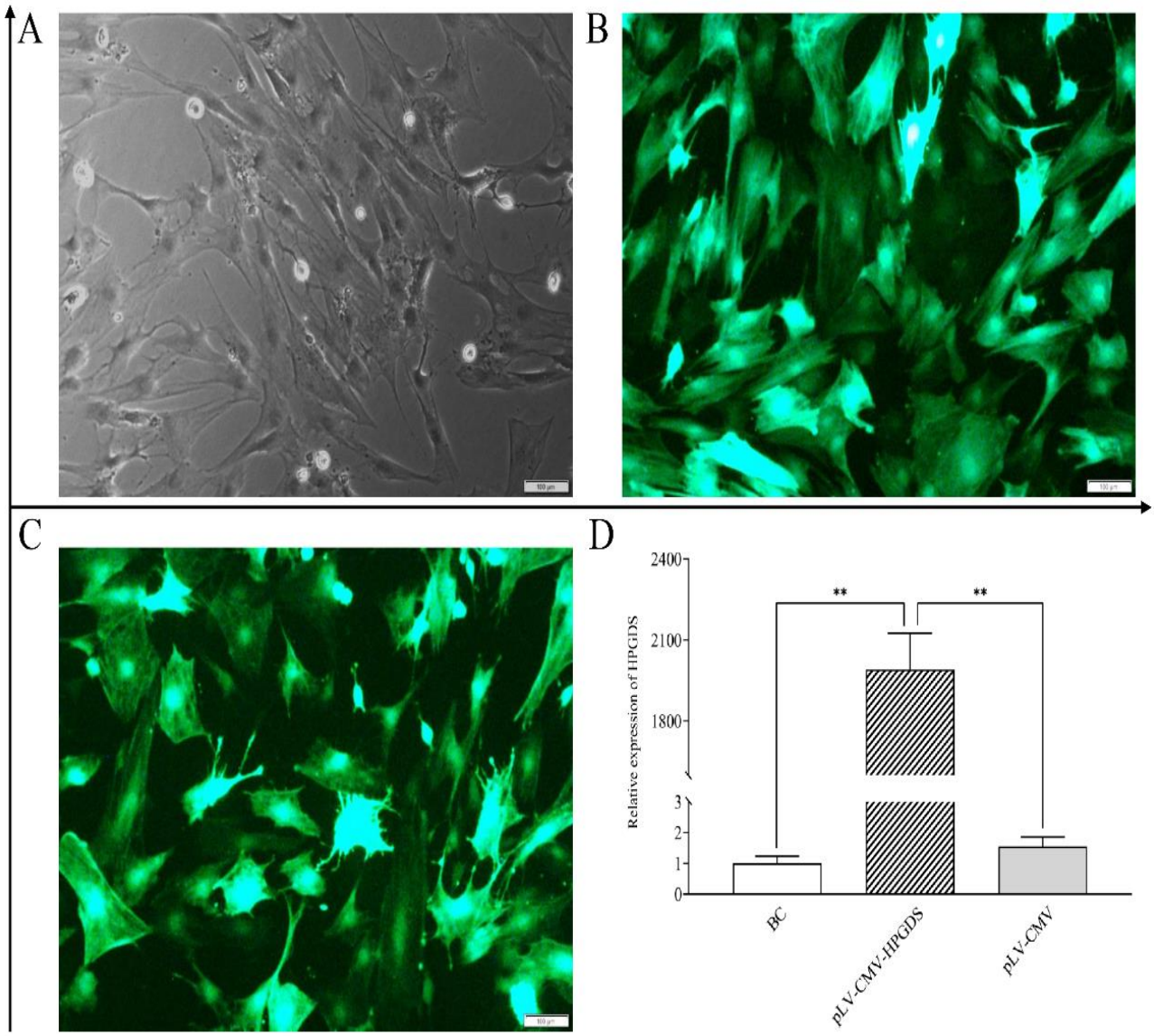

Fig. 4: Results of HPGDS gene overexpression in luteal cells at the optimal MOI value; Lentivirus transfection efficiency of luteal cells observed by fluorescence microscope (100×). A): blank control group (without virus), B): pLV-CMV group (empty vector lentivirus), C): pLV-CMV-HPGDS group (recombinant vector lentivirus), and D: Relative mRNA expression of HPGDS in the above three groups, as determined by qRT-PCR. Note: Blank control group is abbreviated as BC. **Significant differences (P<0.01).

Changes in the expression of key indicators related to HPGDS product transport and biological effects: In the HPGDS overexpression group, ROS concentration was significantly higher (P<0.01; Fig. 6A), and ATP energy metabolic factor ATP6V1B1 mRNA was significantly upregulated (P<0.01; Fig. 6B), while transcriptional regulator CREB mRNA was significantly downregulated (Fig. 6C), than in the EVC and BC groups. Additionally, the PGD_2 transporter SLCO2A1 mRNA (P<0.01; Fig. 6D) and multi-pathway regulatory hub PRKCE mRNA were also significantly upregulated in the HPGDS overexpression group (P<0.01; Fig. 6E). Among PGD_2 receptor genes, DP1 mRNA was also highly significantly upregulated (P<0.01; Fig. 6F), while CRTH2 mRNA was significantly downregulated (P<0.05; Fig. 6G) in the HPGDS overexpression group compared to EVC and BC groups.

Localization and distribution of DP1 and CRTH2 receptors in luteal cells via immunofluorescence: After infecting luteal cells with pLV-CMV and pLV-CMV-HPGDS, immunofluorescence was used to detect PGD_2 receptor localization. The results demonstrated that DP1 receptor was predominantly localized in the nucleus and on the cell membrane, while CRTH2 receptor was localized in the cytoplasm and on the cell membrane. Fluorescence observation showed that DP1 receptor fluorescence was slightly brighter in the HPGDS overexpression group than in the BC and EVC groups (Fig. 7A); subsequent quantification of fluorescence intensity via ImageJ software further confirmed that its intensity in this group was extremely significantly higher than that in both the BC and EVC groups (P<0.01; Fig. 7C). By contrast, no obvious difference in CRTH2 receptor fluorescence intensity was observed between the HPGDS overexpression group, the BC group and the EVC group (Fig. 7B); subsequent quantification of fluorescence intensity values using ImageJ software also showed non-significant difference in CRTH2 receptor fluorescence intensity among three groups (Fig. 7D).

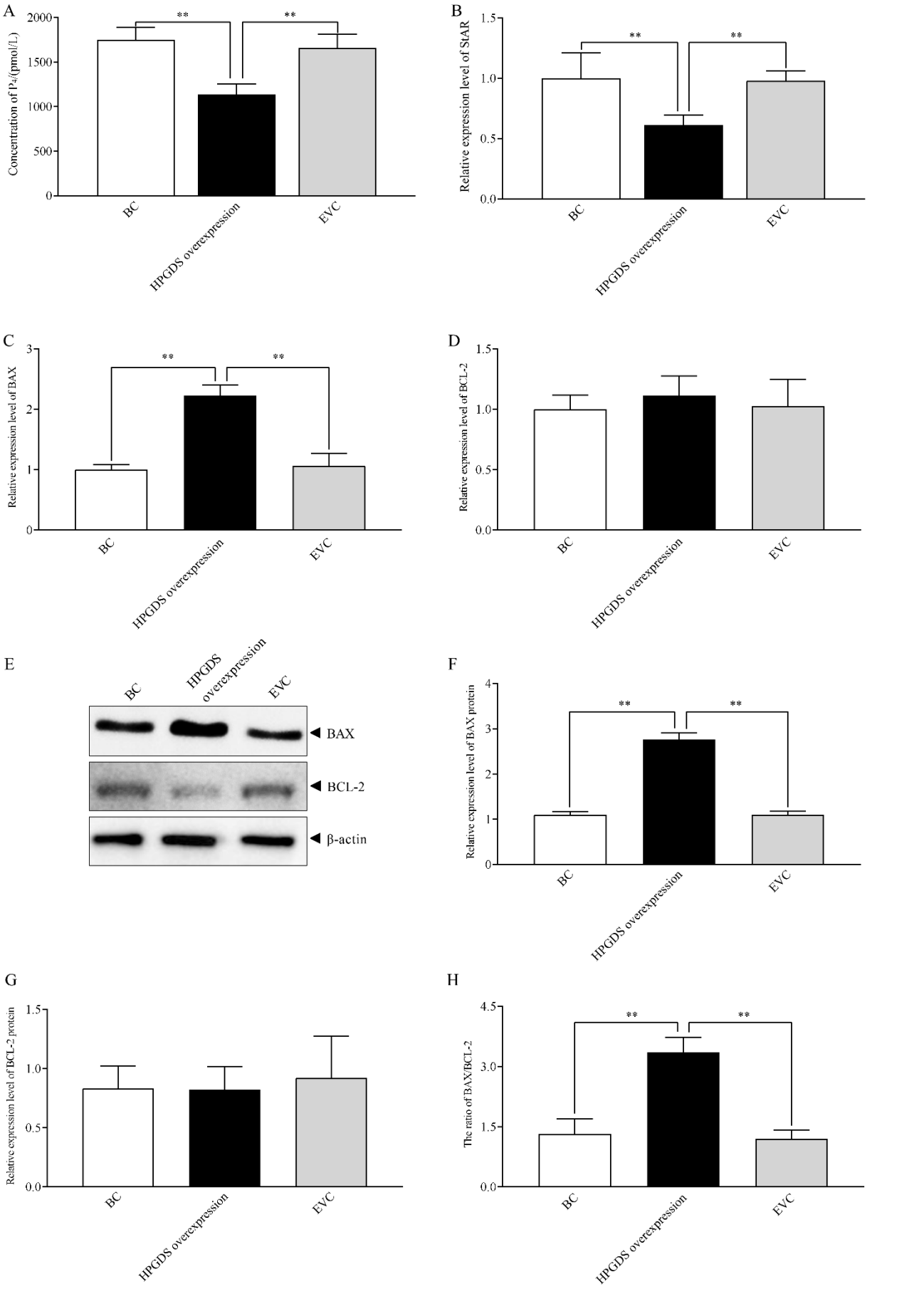

Fig. 5: Changes in the endocrine indicators and expression of apoptosis-related genes in luteal cells (A-D, F-G). E): BAX and BCL-2 protein expressions measured by Western Blot. H): The ratio of relative BAX to BCL-2 protein expressions analyzed using Image J software. **Significant differences ($P<0.01$). Experimental groups: blank control group (without virus, abbreviated as BC), empty control group (pLV-CMV lentivirus, abbreviated as EVC), and experimental group (pLV-CMV-HPGDS lentivirus, abbreviated as HPGDS overexpression).

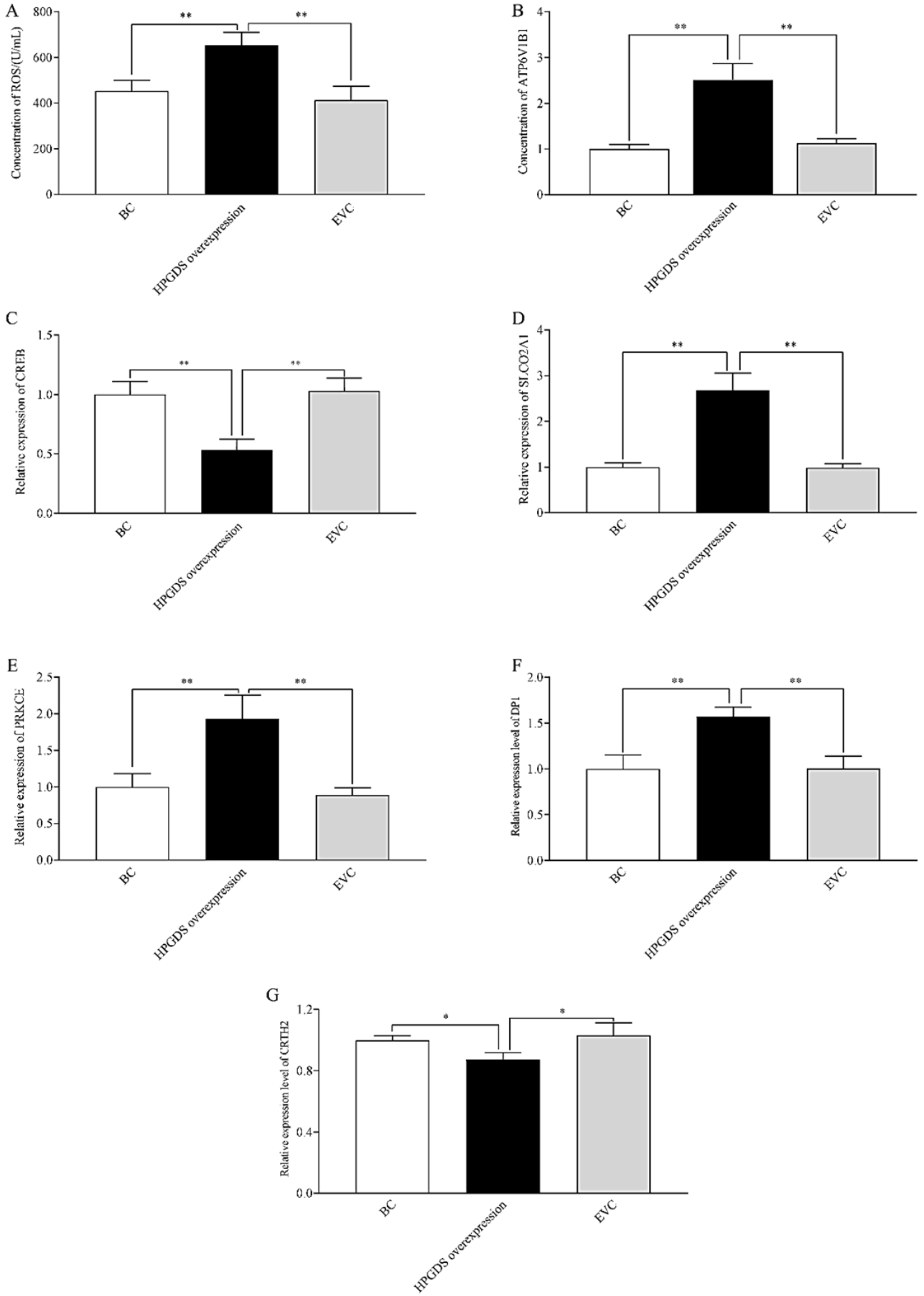

Fig. 6: Changes in the expression of key indicators in the process of material transport and biological effects showing: Concentration of ROS (A), and relative expressions of ATP6V1B1 mRNA (B), CREB mRNA (C), SLCO2A1 mRNA (D), PRKCE mRNA (E), DP1 mRNA (F), and CRTH2 mRNA (G). *Significant differences (P<0.05); **Significant differences (P<0.01). Experimental groups: blank control group (without virus, abbreviated as BC), empty control group (pLV-CMV lentivirus, abbreviated as EVC), and experimental (pLV-CMV- HPGDS lentivirus, abbreviated as HPGDS overexpression).

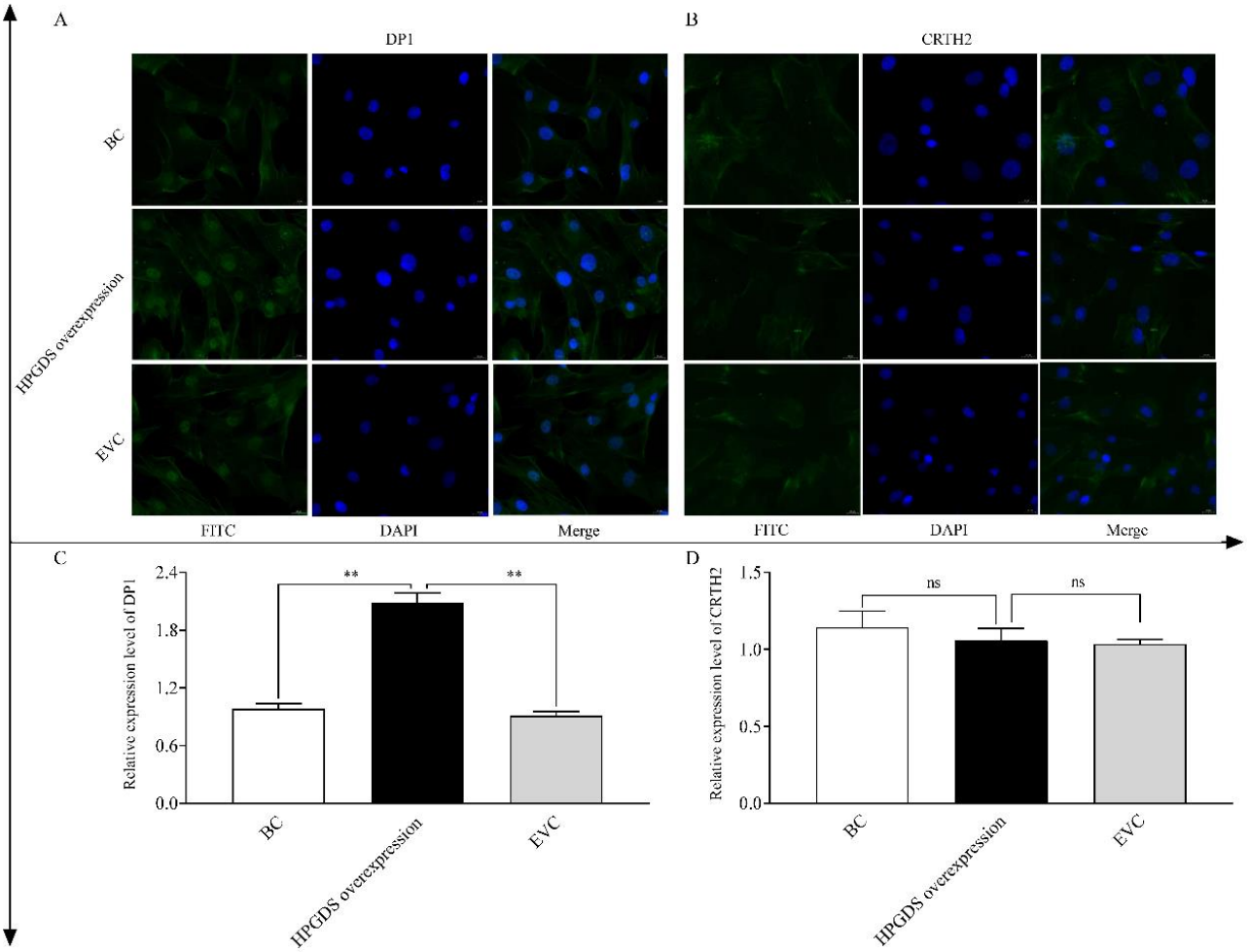

Fig. 7: Localization and distribution of DP1/CRTH2 receptors in luteal cells. A): DP1, and B): CRTH2 immunofluorescence microscopy of the luteal cells. Blue ¼ cell nuclei stained with DAPI; green ¼ PARP1 staining. C): Relative expression levels of DP1, and D): Relative expression levels of CRTH2. **Significant differences (P<0.01). Experimental groups: blank control group (without virus, abbreviated as BC), empty control group (pLV-CMV lentivirus, abbreviated as EVC), and experimental group (pLV-CMV-HPGDS lentivirus, abbreviated as HPGDS overexpression).

DISCUSSION

In the present study, the pLV-CMV-HPGDS lentiviral overexpression vector was constructed, and its successful establishment was confirmed by double enzyme digestion electrophoresis, which yielded fragments of the expected length of the empty plasmid and HPGDS. In the meantime, lentiviral particles with high-titer were obtained through the packaging of 293T cells (Moreira *et al.,* 2021). It was found that lentiviral packaging achieved success in 293T cells, as seen in EGFP-derived green fluorescence, and aligned with previous findings (Mao *et al.,* 2015). Later, lentiviruses were diluted using the limiting dilution. The infection of the 293T cells demonstrated that the titer of the pLV-CMV-HPGDS was 1.4×10^8 TU/ml, and it was enough to obtain the high-titer particles to transduce target cells (particularly primary cells) effectively. Multiplicity of infection (MOI) is described as the number of virus particles in relation to the targeted cells (Rüdiger *et al.,* 2019). Because the MOI values differ when receiving a primary cell infection, it is important to define the best MOI (Kalidasan *et al.,* 2021). In this experiment, the lentivirus was inoculated on the luteal cells at a series of MOI (40, 80, 120, 160, 200, 240), and the best MOI was determined as 160, which is in line with the value given by Moon *et al.* (2000) during a primary cell infection.

Lentiviral vectors enable efficient introduction of target genes into cells for stable expression (Mao *et al.,* 2015; He *et al.,* 2021; Kalidasan *et al.,* 2021). To evaluate the infection efficacy of the pLV-CMV-HPGDS lentiviral vector in primary luteal cells, the optimal MOI (160) was selected in this study for further investigations. Inverted fluorescence microscopy confirmed that luteal cells were successfully infected with pLV-CMV and pLV-CMV-HPGDS lentiviruses. Meanwhile, qRT-PCR results showed that HPGDS expression was significantly upregulated in the pLV-CMV-HPGDS group compared to controls, further confirming that the target gene HPGDS was efficiently overexpressed in primary luteal cells. As a key enzyme in the synthesis of PGD_2, most HPGDS studies focus on diseases such as allergic inflammation (Sio *et al.,* 2023), atopic dermatitis (Nagata *et al.,* 2021), food allergies, and gastrointestinal allergies (Wen *et al.,* 2016). However, according to Michimata *et al.* (2002), HPGDS is widely expressed in female reproductive tissues (trophoblast layer, uterine epithelium, ovaries), suggesting its possible regulatory role in mammalian reproduction.

Corpus luteum is a crucial structure within the reproductive system of female animals, undergoing periodic changes and regulating mammalian reproduction (Wiltbank *et al.,* 2018; de Souza *et al.,* 2024). Luteal function changes are often accompanied by P_4 level

changes. In this experiment, a marked decrease in the concentration of P_4 in the luteal cells was observed following the expression of HPGDS. At the same time, the expression of StAR, an important enzyme of the P_4 synthesis, was also significantly down-regulated. These findings indicate that PGD_2 could control luteal activity similar to that of $PGF_{2\alpha}$, namely decreasing P_4 by inhibiting StAR, thus causing luteal regression (Piotrowska-Tomala *et al.,* 2021; Tavakolikazerooni *et al.,* 2025). Regression of CL includes both functional and structural components. Reduced levels of P_4 can stimulate the processes of luteal cell apoptosis, which consequently causes structural regression (Ogawa *et al.,* 2023). It is worth mentioning that the apoptosis of luteal cells is controlled by the BCL-2 family, and its onset is largely defined by the BAX/BCL-2 ratio (Sozen *et al.,* 2024; Wu *et al.,* 2024). In the current research, BAX expression was evidently increased following the overexpression of HPGDS, without any fluctuations in BCL-2. However, in this case, it is necessary to add that the ratio of BAX/BCL-2 was significantly raised. These findings suggest that PGD_2 causes structural regression through the BAX/BCL-2 apoptosis pathway once functional regression has occurred, which is equivalent to the $PGF_{2\alpha}$-dominated regulatory network (Piotrowska-Tomala *et al.,* 2021; Hojo *et al.,* 2022).

Nevertheless, luteal cell structural regression is frequently mediated by endogenous signals, which include mitochondrial, nuclear, and cell membrane pathways. Mitochondria play an important role in intracellular oxidative metabolism and form the major site of ATP production. They are involved in the regulation of cell death pathways, in addition to being considered important cellular powerhouses (Plewes *et al.,* 2020). Reactive oxygen species (ROS) are major signaling molecules produced during mitochondrial oxidative metabolism. Uncontrolled ROS may cause oxidation of proteins, lipid peroxidation, as well as DNA, which eventually leads to cell death through apoptosis (Villalpando-Rodriguez and Gibson, 2021). The oxidative stress shifts the balance towards cell death, particularly in cells that already have a history of apoptosis, like regressing luteal cells (Hojo *et al.,* 2022). Recent research has shown that apoptosis is an active process that depends on intracellular ATP consumption (Wang *et al.,* 2024), and ATP is necessary to initiate the apoptosis. Our current findings revealed that the level of intracellular ROS of luteal cells was markedly elevated following the overexpression of HPGDS. Meanwhile, ATP6V1B1, which participates in the transport of H^+ and change of energy into ATP, was also markedly upregulated (Han *et al.,* 2023). These results also suggest that PGD_2, in addition to inducing oxidative stress, controls energy metabolism in luteal cells, which in turn could stimulate the process of cell apoptosis and hasten the process of structural regression of CL. The main location of gene transcription is the nucleus and is critical in the synthesis and processing of mRNA (Das *et al.,* 2021). A vital nuclear transcription factor CREB was also highly suppressed in the luteal cells following HPGDS transcription. This pattern was similar to the patterns of expression of StAR and BCL-2. It seems that PGD_2 could coordinate CREB to influence the luteal cell functioning and structure, therefore triggering cascades of downstream regulating mechanisms (Chowdhury *et al.,* 2023). Maximized suppression of these aspects further points to a possible action that the PGD_2 stimulates the luteal cell regression by modifying nuclear transcriptional activity.

Cell membranes function as central platforms for signal transmission and substance transport, which are essential for activating signaling factors and mediating receptor-dependent signal transduction. For instance, protein kinase C (PRKC), a key signaling component, requires translocation from the cytoplasm to the membrane for activation (Hassan *et al.,* 2021), subsequently triggering multiple downstream pathways. Among PRKC subtypes, only PRKCE is upregulated during CL regression (Zorrilla *et al.,* 2009). Additionally, cell membranes widely express PG transporters and their family receptors. The SLCO2A1 functions as a key PG transporter that regulates the distribution of local and systemic PGs (Nakanishi *et al.,* 2021). DP1 and CRTH2 constitute the dual-receptor system for PGD_2, which modulates the fate of target cells. Our results showed that PRKCE and SLCO2A1 were obviously upregulated in luteal cells after HPGDS overexpression. However, in the PGD_2 dual-receptor system, only DP1 exhibited a striking upregulation. Similarly, immunofluorescence result also showed that DP1 fluorescence intensity was significantly enhanced after HPGDS overexpression. These results indicate that PGD_2 may be transported by SLCO2A1 and then preferentially bind to DP1. Ultimately, it may engage in the aforementioned multi-pathway regulation through PRKCE activation (García-Solaesa *et al.,* 2014).

Overall, the findings of this study are consistent with earlier reports on $PGF_{2\alpha}$ (Shirasuna *et al.,* 2012). Specifically, PGD_2 regulates luteal cells via both the PKC/PRKCE-P_4 pathway and the PKC/PRKCE-apoptosis pathway (Mcguire *et al.,* 1994), ultimately initiating functional regression and structural extinction of luteal cells. Although the present study has delineated the intracellular effects of HPGDS overexpression at the cellular level, the lack of quantitative data on PGD_2 concentrations has precluded a comprehensive mechanistic interpretation of these observations. This limitation, however, highlights a critical avenue for future research, and we aim to systematically elucidate the regulatory mechanism through which PGD_2 modulates CL lifespan in the future.

Conclusions: In summary, after HPGDS overexpression, PGD_2 might preferentially binds to the DP1 receptor and converts extracellular signals into intracellular signals via the PKC/PRKCE pathway. Initially, the nuclear transcription factor CREB is downregulated, which concurrently reduces StAR expression. The reduced StAR expression lowers P_4 levels, thereby initiating functional regression of luteal cells. Subsequently, the mitochondrial apoptosis pathway is activated by an increased BAX/BCL-2 ratio, effectively shifting the balance toward cell death. Meanwhile, intracellular rise of ROS levels further accelerates the BAX-mediated apoptosis pathway and disrupts the ATP-ADP balance by altering the mitochondrial H^+ concentration gradient, thus promoting structural regression of luteal cells. Ultimately, these combined effects lead to luteal cell extinction.

Animal ethics: Ovarian tissues used in this study were abattoir by-products from commercially slaughtered food-

producing animals. All procedures complied with China's NY/T 3469-2019 Operating Procedures of Livestock and Poultry Slaughtering-Sheep and Goat and the Regulations on the Administration of Experimental Animals (Decree No. 676, State Council). No animals were sacrificed specifically for this study, so institutional animal ethics approval was not required.

Authors contribution: HY, LG, GFW, LF and XWD designed the experiments. HY, RL, JMW, LHL, LCL, LF and ZKW collected samples. HY, JMW, HHX and XWD analyzed the data. HY and RL drafted the manuscript. HY revised the manuscript. All authors reviewed and approved the final version of the manuscript.

Funding sources: This work was supported by Strategic Cooperation Project between Chongqing Municipality and Chinese Academy of Agricultural Sciences (23311), Chongqing Municipal College Student Innovation and Entrepreneurship Training Program (S202510635336), Fundamental Research Funds for the Central Universities (SWU-KT22015).

Conflicts of interest: The authors declare no conflict of interest.

Acknowledgments: We are grateful to all the members of the laboratory for their help in sampling and performing the experiments.

REFERENCES

Abaandou L, David Q and Joseph S, 2021. Affecting HEK293 cell growth and production performance by modifying the expression of specific genes. Cells 10:1667.

Ahmad AS, Ottallah H, Maciel CB, *et al*., 2019. Role of the L-PGDS-PGD2-DP1 receptor axis in sleep regulation and neurologic outcomes. Sleep 42(6):zsz073. doi: 10.1093/sleep/zsz073.

Berisha B, Schams D, Rodler D, *et al*., 2018. Changes in the expression of prostaglandin family members in bovine corpus luteum during the estrous cycle and pregnancy. Mol Reprod Dev 85:622-34.

Bonnin P, Huynh L, L'Haridon R, *et al*., 1999. Transport of uterine PGF2α to the ovaries by systemic circulation and local lymphovenous-arterial diffusion during luteolysis in sheep. Reproduction 116(1):199-210.

Charpigny G, Reinaud P, Créminon C, *et al*., 1999. Correlation of increased concentration of ovine endometrial cyclooxygenase 2 with the increase in PGE2 and PGD_2 in the late luteal phase. Reproduction 117(2):315-24.

Chen F, Wen X, Lin P, *et al*., 2018. Activation of CREBZF increases cell apoptosis in mouse ovarian granulosa cells by regulating the ERK1/2 and mTOR signaling pathways. Int J Mol Sci 19(11):3517.

Chen Q, Sun W, Jin L, *et al*., 2024. Overexpression of Kdm6b induces testicular differentiation in a temperature-dependent sex determination system. Zool Res 45(5):1108.

Chowdhury MAR, An J and Jeong S, 2023. The pleiotropic face of CREB family transcription factors. Mol Cells 46(7):399-413.

Das S, Vera M, Gandin V, *et al*., 2021. Intracellular mRNA transport and localized translation. Nat Rev Mol Cell Biol 22(7):483-504.

de souza MCB, Antunes RA, de Souza MM, *et al*., 2024. Corpus luteum and progesterone in embryo transfer cycles: current challenges of different luteal phase support protocols. JBRA Assist Reprod 28(2):211-14.

Fang X, Xia W, Li S, *et al*., 2022. SIRT2 is critical for sheep oocyte maturation through regulating function of surrounding granulosa cells. Int J Mol Sci 23(9):5013.

García-Solaesa V, Sanz-Lozano C, Padrón-Morales J, *et al*., 2014. The prostaglandin D2 receptor (PTGDR) gene in asthma and allergic diseases. Allergol Immunopathol (Madr) 42(1):64-8.

Gong Z, Mao W, Jin F, *et al*., 2023. Prostaglandin D2 regulates Escherichia coli-induced inflammatory responses through TLR2, TLR4, and NLRP3 in macrophages. Prostagl Other Lipid Mediat 169:106772.

Han GH, Yun H, Chung JY, *et al*., 2023. High ATP6V1B1 expression is associated with poor prognosis and platinum-based chemotherapy resistance in epithelial ovarian cancer. Oncol Rep 49(5): 102. doi: 10.3892/or.2023.8539.

Han Y, Yao R, Yang Z, *et al*., 2022. Interleukin-4 activates the PI3K/AKT signaling to promote apoptosis and inhibit the proliferation of granulosa cells. Exp Cell Res 412(1):113002.

Hassan Z, Kumar ND, Reggiori F, *et al*., 2021. How viruses hijack and modify the secretory transport pathway. Cells 10(10):2535.

He X, He Q, Yu W, *et al*., 2021. Optimized protocol for high-titer lentivirus production and transduction of primary fibroblasts. J Basic Microbiol 61:430-42.

Hojo T, Skarzynski DJ and Okuda K, 2022. Apoptosis, autophagic cell death, and necroptosis: different types of programmed cell death in bovine corpus luteum regression. J Reprod Dev 68:355-60.

Kalidasan V, Ng WH, Ishola OA, *et al*., 2021. A guide in lentiviral vector production for hard-to-transfect cells, using cardiac-derived c-kit expressing cells as a model system. Sci Rep 11(1):19265.

Li Y, Kim WM, Kim SH, *et al*., 2021. Prostaglandin D2 contributes to cisplatin-induced neuropathic pain in rats via DP2 receptor in the spinal cord. Korean J Pain 34:27-34.

Mao Y, Yan R, Li A, *et al*., 2015. Lentiviral vectors mediate long-term and high efficiency transgene expression in HEK 293T cells. Int J Med Sci 12:407.

Mcguire WJ, Juengel JL and Niswender GD, 1994. Protein kinase C second messenger system mediates the anti-steroidogenic effects of prostaglandin F2α in the ovine corpus luteum in vivo. Biol Reprod 51:800-806.

Michimata T, Tsuda H, Sakai M, *et al*., 2002. Accumulation of CRTH2-positive T-helper 2 and T-cytotoxic 2 cells at implantation sites of human decidua in a prostaglandin D2-mediated manner. Mol Hum Reprod 8:181-87.

Moon SH, Gilbertson LG, Nishida K, *et al*., 2000. Human intervertebral disc cells are genetically modifiable by adenovirus-mediated gene transfer: implications for the clinical management of intervertebral disc disorders. Spine 25:2573-79.

Moreira AS, Cavaco DG, Faria TQ, *et al*., 2021. Advances in lentivirus purification. Biotechnol J 16:2000019.

Nagata N, Hamasaki Y, Inagaki S, *et al*., 2021. Urinary lipid profile of atopic dermatitis in murine model and human patients. FASEB J 35(11):e21949.

Nakanishi T, Nakamura Y and Umeno J, 2021. Recent advances in studies of SLCO2A1 as a key regulator of the delivery of prostaglandins to their sites of action. Pharmacol Therapeut 223:107803.

Neglia G, Vecchio D, Russo M, *et al*., 2012. Efficacy of PGF2α on pre-ovulatory follicle and corpus luteum blood flow. Reprod Domest Anim 47:26-31.

Ochoa JC, Penagaricano F, Baez GM, *et al*., 2018. Mechanisms for rescue of corpus luteum during pregnancy: gene expression in bovine corpus luteum following intrauterine pulses of prostaglandins E1 and F2α. Biol Reprod 98:465-79.

Ogawa M, Kitamoto J, Takeda T, *et al*., 2023. Bisphenol A prevents MCF-7 breast cell apoptosis via the inhibition of progesterone receptor transactivation. J Biochem Mol Toxicol 37:e23367.

Pate JL and Hughes CHK, 2023. Luteal prostaglandins: mechanisms regulating luteal survival and demise in ruminants. Animal 17(Suppl 1):100739.

Piotrowska-Tomala KK, Jonczyk AW, Kordowitzki P, *et al*., 2021. The effect of basic fibroblast growth factor 2 on the bovine corpus luteum depends on the stage of the estrous cycle and modulates prostaglandin F2α action. Animal 15(1):100048.

Plewes MR, Hou X, Talbott HA, *et al*., 2020. Luteinizing hormone regulates the phosphorylation and localization of the mitochondrial effector dynamin-related protein-1 (DRP1) and steroidogenesis in the bovine corpus luteum. FASEB J 34:5299-5316.

Rüdiger D, Kupke SY, Laske T, *et al*., 2019. Multiscale modeling of influenza A virus replication in cell cultures predicts infection dynamics for highly different infection conditions. PLoS Comput Biol 15(2):e1006819.

Satoh H, Terashima R, Kawaminami M, et al., 2021. Prostaglandins F2α and E2 in rat placenta and fetal membrane: a comprehensive immunohistochemistry of their synthetic enzymes and in vivo tissue levels during normal pregnancy. J Vet Med Sci 83:1443-1447.

Shirasuna K, Akabane Y, Beindorff N, *et al*., 2012. Expression of prostaglandin F2α (PGF2α) receptor and its isoforms in the bovine corpus luteum during the estrous cycle and PGF2α-induced luteolysis. Domest Anim Endocrinol 43:227-38.

Sio YY, Shi P, Matta SA, *et al*., 2023. Functional polymorphisms of the arachidonic acid pathway associate with risks and clinical outcomes of allergic diseases. Int Arch Allergy Immunol 184:609-23.

Sozen ME, Savas HB and Cuce G, 2024. Protective effects of selenium against acrylamide-induced hepatotoxicity in rats. Pak Vet J 44:274-79.

Tan J, Xu W, Lei L, *et al*., 2020. Inhibition of aurora kinase a by alisertib reduces cell proliferation and induces apoptosis and autophagy in huh-6 human hepatoblastoma cells. Onco Targets Ther 13:3953-63.

Tavakolikazerooni H, Tariq M, Ullah S, *et al*., 2025. Melatonin modulates necroptosis and enhances antioxidant defense during PGF-induced luteal regression in heat-exposed rats. Pak Vet J 45:205-15.

Tippenhauer CM, Steinmetz I, Heuwieser W, *et al*., 2021. Effect of dose and timing of prostaglandin F2α treatments during a 7-d Ovsynch protocol on progesterone concentration at the end of the protocol and pregnancy outcomes in lactating Holstein cows. Theriogenology 162:49-58.

Ullah MA, Rittchen S, Li J, *et al*., 2024. Dual therapy with corticosteroid ablates the beneficial effect of DP2 antagonism in chronic experimental asthma. Nat Commun 15:10253.

Villalpando-Rodriguez GE and Gibson SB, 2021. Reactive oxygen species (ROS) regulates different types of cell death by acting as a rheostat. Oxid Med Cell Longev1:9912436.

Wang J, Yang Y, Ma J, *et al*., 2025. Molecular mechanism of N-Acetylcysteine regulating proliferation and hormone secretion of granulosa cells in sheep. Reprod Domest Anim 60(1):e70006.

Wang X, Xu Z, Zhuang Y, *et al*., 2024. Evaluating the impact of Trimetadizine on myocardial ischemia-reperfusion injury through mitochondrial ATP pathway in rats. Pak Vet J 44:715-20.

Wang Y, Wu C, Zhou J, *et al*., 2022. Overexpression of estrogen receptor β inhibits cellular functions of human hepatic stellate cells and promotes the anti-fibrosis effect of calycosin via inhibiting STAT3 phosphorylation. BMC Pharmacol Toxicol 23(1):77.

Wen T, Rothenberg ME and Wang YH, 2016. Hematopoietic prostaglandin D synthase: Linking pathogenic effector CD4+ TH2 cells to pro-eosinophilic inflammation in patients with gastrointestinal allergic disorders. J Allergy Clin Immunol 137:919-21.

Wiltbank MC, Meidan R, Ochoa J, *et al*., 2018. Maintenance or regression of the corpus luteum during multiple decisive periods of bovine pregnancy. Anim Reprod 13:217-33.

Wu Z, Cui Y, Mao W, *et al*., 2024. Bufalin Promotes Apoptosis and Autophagy Through the JAK-STAT Signaling Pathway in Myeloid Leukemia. Pak Vet J 44:1142-1152.

Yang H, Fu L, Li L, *et al*., 2023. miR-665 overexpression inhibits the apoptosis of luteal cells in small ruminants suppressing HPGDS. Theriogenology 206:40-48.

Zhu L, Shahbaz GM, Sun H, *et al*., 2025. Expression dynamics and estrogen response of estrogen receptors in Duolang sheep during puberty. Genes 16(7):731.

Zorrilla LM, Irvin MS and Gadsby JE, 2009. Protein kinase C isoforms in the porcine corpus luteum: temporal and spatial expression patterns. Domest Anim Endocrinol 36:173-85.